nature communications

Article | Article in Press

https://doi.org/10.1038/s41467-026-79122-3

Combing-triggered electrostimulation synchronizing deep delivery for rapid hair regrowth in androgenetic alopecia

Received: 28 January 2026

Accepted: 13 October 2026

Published online: 03 November 2026

Check for updates

Feng Liu[1,2,3,8], Fuqi Yao[1,2,3,8], Hong Sun[4,8], Chengbao Wu[5], Bing Liu[6], Yihang Tong[1,2,3], Chunhong Dai[2], Han Wu[1,2,3], Ruowen Zhang[1,2,3], Dedong Yin[1,2,3], Xiaowei Xiang[1,2,3], Tianhang Feng[1,2,3], Liye Liu[5], Peng Zhang[1,2,3], Nan Wu[6], Yanli Jiao[7] ✉, Zaizai Dong[1,3] ✉ & Lingqian Chang[1,3,5] ✉

Androgenetic alopecia affects over 1.5 billion individuals, causing progressive hair loss with psychological and quality-of-life burdens. Current pharmacological treatment for androgenetic alopecia faces challenges due to systemic side effects from oral medications or limited efficacy of topical applications. Herein we develop a comb-shaped bioelectronic system, named "Detangle", for efficient androgenetic alopecia treatment during daily hair combing. This system features electronic teeth embedded with height-differentiated electrodes and integrated drug-loading modules, which generate an enhanced electric field penetrating up to ~9 times deeper into hair follicle regions than conventional external application. We show that the localized electric field synchronizes electro-stimulating hair follicles, and electro-delivering vascular endothelial growth factor A encoding plasmid and steroid 5-alpha-reductase 2 targeting siRNA into follicular cells to promote angiogenesis and suppress androgen synthesis. Through the synergistic regulation of cellular metabolism, the system significantly increases hair restoration efficacy in an androgenetic alopecia mouse model, improving the outcome from ~70% to nearly 100% within one month compared to conventional topical minoxidil treatment. The Detangle system proves safe and effective for deep tissue delivery in dermatology.

Androgenetic alopecia (AGA) remains a global health issue affecting approximately 1.5–2 billion people. It features hair follicle miniaturization caused by abnormal upregulation of androgens, which imposes significant psychological distress and daily-life burden[1–4]. Current clinical treatments face significant limitations: oral drugs are recognized for a lack of specificity and may cause systemic side effects, while external application has limited ability to penetrate the skin barrier and reach the deep follicles[5–8]. Microneedle-mediated drug delivery could enhance localized delivery efficiency by piercing into epidermis layers[9–11]. However, their invasive nature risks follicular

[1]School of Engineering Medicine, Beihang University, Beijing, China. [2]School of Biological Science and Medical Engineering, Beihang University, Beijing, China. [3]Qingdao Research Institute, Beihang University, Qingdao, China. [4]Beijing Chest Hospital, Capital Medical University & Beijing Tuberculosis and Thoracic Tumor Research Institute, Translational Medicine Center, Beijing, China. [5]School of Biomedical Engineering, Anhui Medical University, Hefei, China. [6]State Key Laboratory of Molecular Oncology, Key Laboratory of Carcinogenesis and Translational Research (Ministry of Education/Beijing), Department of Thoracic Surgery II, Peking University Cancer Hospital and Institute, Beijing, China. [7]Department of Biomedical Engineering, Institute of Digital Medicine, Hong Kong Institute for Clean Energy, City University of Hong Kong, Hong Kong, China. [8]These authors contributed equally: Feng Liu, Fuqi Yao, Hong Sun. ✉e-mail: yl.jiao@cityu.edu.hk; dongzaizai@buaa.edu.cn; lingqianchang@buaa.edu.cn

damage and hampers large-area application. Additionally, skin adhesion-based operation is severely impaired by the presence of hair, rendering them impractical in sustaining hair growth over the long term[12–14]. Safe and efficient delivery remains the key to the treatment outcome of AGA.

Here, we report "Detangle" (a name inspired by the animated film *Tangled*), a comb-shaped device engineered for AGA treatment. The system employs a control circuit to generate pulsed electric fields and integrates two types of electronic teeth with differential heights as electrodes that, triggered by the combing action, raise the skin to generate a 2.63 times stronger electric field compared to that produced by aligned electrodes. This enhanced field creates sufficient transmembrane potential for the subsequent delivery of regulatory molecules into follicular cells, significantly increasing their intracellular uptake efficiency by up to 3.4-fold. Through the synergistic effect that electrostimulation regulates cellular metabolism, while co-delivery of VEGFA plasmid (to enhance perifollicular vascularization) and SRD5A2 siRNA (to inhibit androgen secretion) amplifies the therapeutic effect, hair growth recovers nearly 100% within a month in the AGA mouse model, significantly surpassing the ~70% recovery rate of conventional topical minoxidil treatment methods in the same model. Detangle represents a non-invasive strategy synergizing electrostimulation with electric delivery for enhanced AGA treatment.

Results

Design of the Detangle system

To customize the Detangle system for targeted treatment of AGA, a fundamental study was conducted to identify differentially expressed molecules between AGA and control mice (Fig. S1a–j). Comparative analysis shows 2903 upregulated and 2770 downregulated molecules that are mostly associated with cellular metabolic pathways. According to the existing literature, these pathways can be modulated by electrostimulation, which inspired the integration of electrotherapy into the Detangle system[15–20]. However, we observed that conventionally aligned electrodes exhibit limited penetration strength into the scalp (<98.89 V/m). In contrast, leveraging the scalp's natural compliance in conjunction with electrodes of differential heights significantly enhances the electric field strength (260.37 V/m) (Fig. S2a–c). Guided by these principles while considering daily grooming needs, we designed the Detangle system with a comb-like configuration that incorporates two types of electrode-embedded teeth arranged with alternating height differences (Fig. 1a–g and Fig. S3a–d).

Moreover, the electric field used for electrostimulation can drive charged molecules from the skin surface into deeper tissue layers[21,22]. The system generates a voltage gradient exceeding 0.2 V around hair follicles, suggesting that a sufficient transmembrane potential is established to reversibly open cell membranes and enable intracellular molecular delivery (Fig. S2a, b)[21,23]. To further enhance the therapeutic efficacy, we integrated molecular delivery capability into the Detangle system. For this purpose, the shorter teeth of Detangle system, designated as drug-loading modules, are preloaded with therapeutic molecules, such as low-molecular-weight SRD5A2 siRNA (~21 nt) and macromolecular VEGFA plasmid (~5.2 kb) (Fig. 1g). These two molecules can not only verify the system's universal delivery capability but also synergistically enhance hair follicle cell regeneration by upregulating VEGFA to promote angiogenesis and downregulating SRD5A2 to suppress the synthesis of dihydrotestosterone (DHT, the primary human androgen)[24–29]. Moreover, the tips of drug-loading modules feature a ball-based release mechanism, functionally analogous to a ballpoint pen, that enables contact-triggered molecular deployment (Fig. 1c).

During operation, the height difference between adjacent teeth generates a directional electric field spanning from the teeth of drug-loading modules to the teeth of longer electrode modules (Fig. 1f and Fig. S2a–c). The electric field drives transdermal transport of the released regulatory molecules and promotes their delivery to the deep follicular regions under a low voltage, ensuring both the safety and efficacy of the process[30,31]. The synergistic combination of electrostimulation and molecular regulation in the Detangle system effectively reverses the androgen-induced suppression of hair follicle activity, leading to rapid recovery of hair growth.

AGA treatment by electrostimulation

To evaluate Detangle-mediated electrostimulation for AGA treatment (e.g., safety and treatment efficacy), both theoretical modeling and experimental validation were conducted (Fig. 2a). Electric field simulations show that the Detangle electrode array generated an electric field intensity of approximately 260.37 V/m surrounding the follicular regions (Fig. S2a, c). Electrostimulation (ES) at this intensity produced no significant changes in body weight or inflammatory cytokine levels, suggesting the safety of the applied electrical parameters (Fig. 2b and Fig. S4a–c). Furthermore, the long-term safety of electrical stimulation was evaluated at the epidermal, cellular, and molecular levels[30,32–36]. The absence of notable epidermal changes, along with unaltered levels of cellular damage markers (Ki67 and Tunel) and nerve injury-associated factors (PGP9.5, CALCA, and MCP7), collectively supports the high safety of electrical stimulation (Fig. S5a–f).

The therapeutic efficacy was further validated using an AGA mouse model (Fig. 2c–l). The model was characterized by key AGA features, including hair loss, decreased hair follicles, aberrant androgen and receptor signaling, decreased microcirculation, and perifollicular inflammation[37–40]. The presence of features consistent with AGA confirmed successful model establishment (Fig. 2c and Fig. S6a–k). Based on hair-growth results, the electrically stimulated (AGA+ES) group exhibits significantly enhanced hair growth (hair coverage: 39.52 *vs.* 0.90; hair cycle score: 2.60 *vs.* 0.60) and an increased number of hair follicles (151 *vs.* 49.5) compared to the non-stimulated control (AGA) group (Fig. 2c-h). Additionally, the increased local blood flow, blood vessels, and vascular marker CD31 further demonstrated the efficacy of electrical stimulation (Fig. 2i–k and Fig. S7). Moreover, elevated expression of follicular-activation marker CD34 (5.80-fold) was also observed in the electrically stimulated group (Fig. 2j, l). Together, these results demonstrate that electrostimulation via the Detangle system promotes hair growth and follicle regeneration in a safe and effective manner.

To elucidate the mechanism underlying electrostimulation-induced therapeutic effect, we compared protein expression between electrically stimulated and non-stimulated groups. Analysis results reveal that electrically stimulated skin exhibits up-regulation of 673 proteins and down-regulation of 777 proteins relative to non-stimulated controls, with the majority of differentially expressed proteins enriched in cellular metabolic pathways (accounting for eight of the top-ten enriched terms in GO analysis) (Fig. 2m, n and Fig. S8a–i). Based on KEGG enrichment analysis, the amino sugar and nucleotide sugar metabolism pathway exhibited the most significant differences (Fig. 2o-p). Within this signaling pathway, the PGM3 protein was validated to play a major role in linking amino sugar metabolism to the downstream Wnt/β-catenin pathway, which is the main regulatory pathway for hair follicle regeneration[4,37,41,42] (Fig. 2q, r). This result suggests that electrical stimulation promotes hair regeneration by upregulating PGM3 to activate the Wnt/β-catenin pathway.

In addition, the DHT levels progressively decreased with increasing frequency of electrical stimulation, indicating that electrostimulation exerts a direct therapeutic effect (Fig. 2s). To investigate whether this effect arises from microenvironmental modulation or indirectly from anagen entry, we analyzed markers of microenvironmental status (TNF-α, IL-1β, IL-6) and hair follicle anagen entry (Ki67). The results showed a progressive decrease in the expression of inflammatory cytokines with increasing numbers of electrostimulation sessions (Fig. 2t–v). Notably, Ki67 expression remained stable during

https://doi.org/10.1038/s41467-026-79122-3

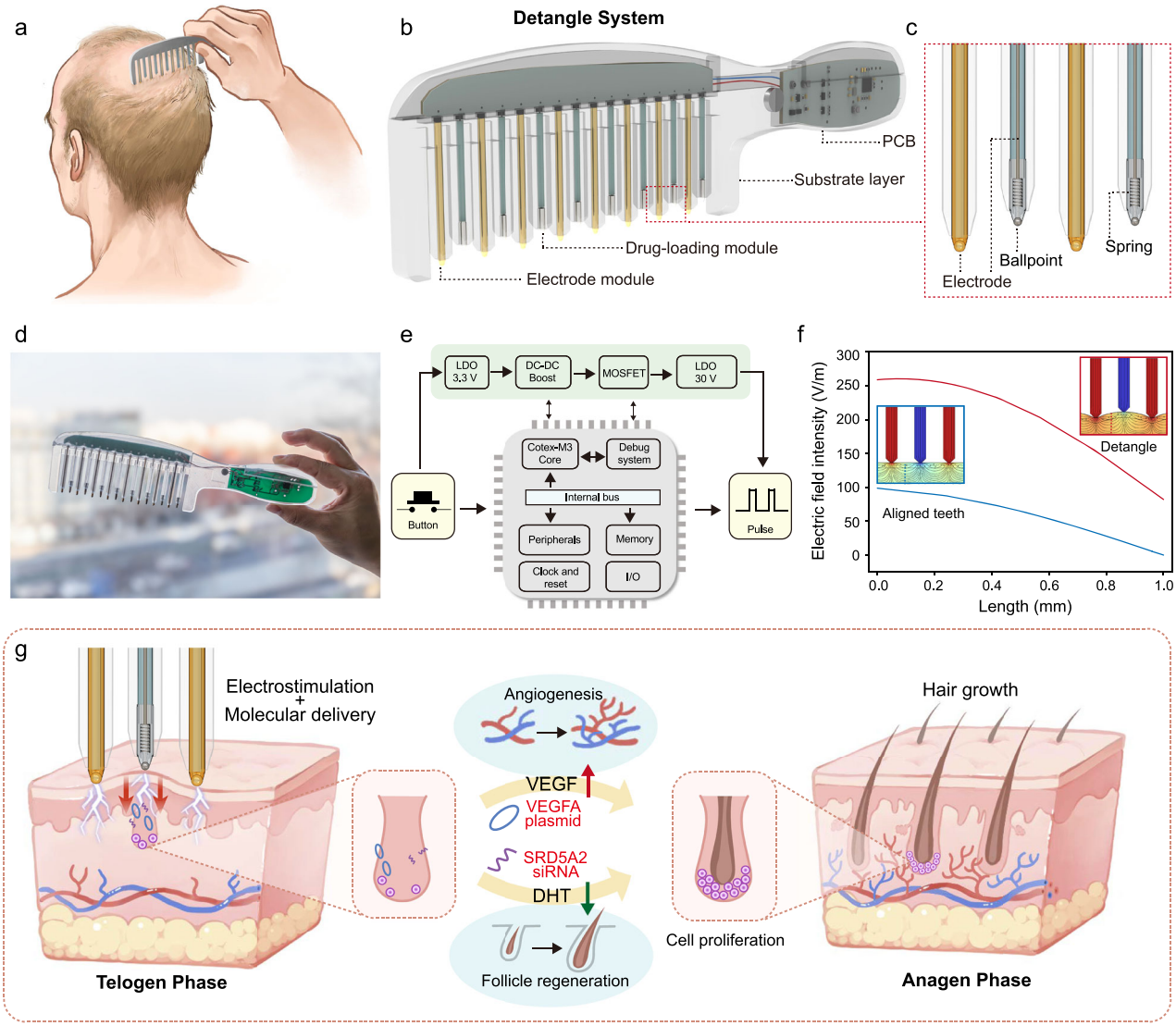


Fig. 1 | Detangle system for enhanced efficacy of AGA through electrostimulation-assisted deep molecular delivery. a Schematic illustration of the Detangle system for enhanced efficacy of AGA in daily operation. **b** Schematic of the structure of the Detangle system. PCB, printed circuit board. **c** Detailed illustration of the drug-loading module and electrode module in the Detangle system. **d** Physical diagram of the Detangle system. **e** Schematic diagram of the circuit in the Detangle system. **f** Comparison of electric field intensity in the Detangle system and aligned teeth. **g** Detangle system promotes hair growth through deep delivery of regulatory molecules into hair follicle cells. The VEGFA plasmid stimulates angiogenesis around hair follicles, and the SRD5A2 siRNA suppresses DHT synthesis.

the initial phase of electrostimulation and did not increase until after two stimulation sessions (Fig. S9). These findings suggest that in the early phase of electrostimulation, DHT suppression is primarily achieved through alterations in the local microenvironment. As the microenvironment recovers and hair follicles gradually enter the anagen phase, both microenvironmental improvement and anagen entry synergistically suppress DHT production in the later phase of treatment.

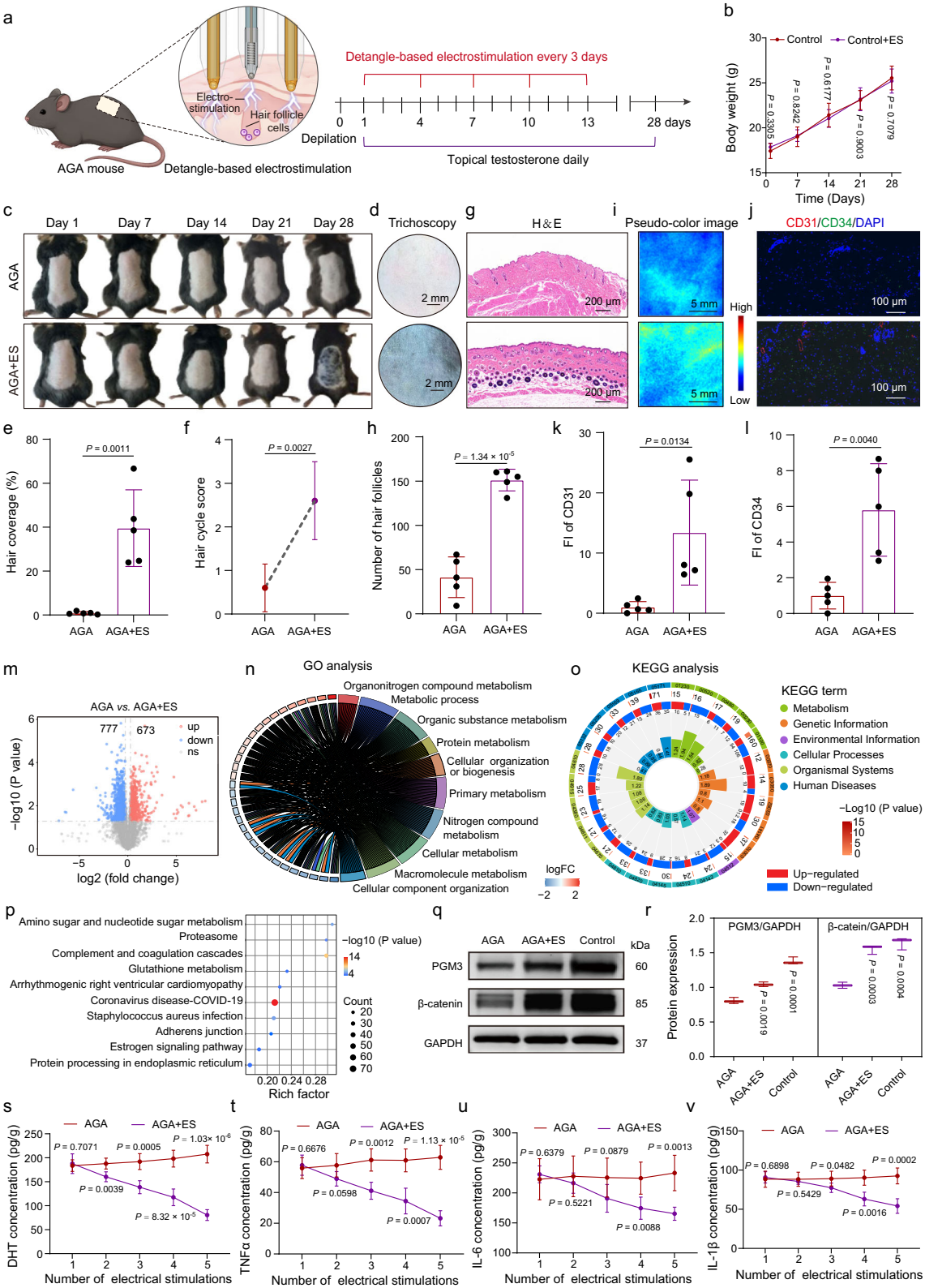
Detangle system for in vivo delivery

To improve therapeutic outcomes for AGA, we utilized the Detangle system to deliver regulatory molecules into the hair-follicle region. Experimental validation shows that the system delivers surface-applied molecules to a depth of ~660 μm in the skin within one second, significantly deeper than conventional external application (~74 μm) and aligned teeth (~250 μm) (Fig. 3a–d). At this depth, the induced transmembrane potential exceeds 0.7 V, enabling efficient electroporation-mediated delivery into follicular cells (Fig. 3e)[19,21,43].

For the delivered regulators, we selected the VEGFA plasmid, which enhances local metabolism by promoting angiogenesis, and the SRD5A2 siRNA, which suppresses androgen synthesis through the pathway by suppressing the synthesis of DHT (Fig. 3f)[5,25,40,44]. Following delivery, qPCR analysis confirmed significantly enhanced levels of *VEGFA* mRNA and SRD5A2 siRNA in skin tissues (Fig. 3g, h). This substantial increase, which markedly exceeded levels in the control, external application, and aligned teeth groups, confirms the Detangle system's capability for effective deep-tissue delivery.

Furthermore, under realistic conditions, the delivery area on the scalp exhibits blurred boundaries, raising the possibility of overlapping application. To assess the safety of such applications, repeated delivery was performed at the same skin site. Macroscopic skin appearance, histological evaluation (H&E staining), and inflammatory markers show no significant differences between repeatedly delivered and non-delivered groups, demonstrating the high safety of the Detangle system (Fig. 3i–l).

https://doi.org/10.1038/s41467-026-79122-3



Detangle system for AGA treatment

To further validate Detangle-mediated therapy, the AGA mice were treated with Detangle system delivering VEGFA plasmid (G2), SRD5A2 siRNA (G3), and both (G4) (Fig. 4a). Molecular delivery via the Detangle system results in significant changes of both gene and protein expression in the skin of AGA mice, indicating the intended intervention through the regulatory pathways (Fig. 4b–e). Furthermore, this regulation achieves stable and durable biological responses with increasing treatment sessions (Fig. S10). Macroscopic and trichoscopy evaluation of hair growth shows that delivery of either VEGFA plasmid or SRD5A2 siRNA alone promotes hair growth compared with the untreated control (Fig. 4f, g). Noticeably, co-delivery of

Fig. 2 | Detangle system for AGA treatment by electrostimulation. a A schematic diagram of the Detangle system for AGA mouse treatment through electrostimulation. The AGA mouse model was established by daily topical application of testosterone for 28 consecutive days. **b** Body weight monitoring during the treatment of mice with electrostimulation. Control, non-stimulated normal mice. Control+ES, electrically stimulated normal mice. **c** Representative photographs showing hair growth in AGA mice with or without electrostimulation treatment. **d** Trichoscopy images of mouse skin tissue with and without electrical stimulation. Scale bar = 2 mm. Comparative quantification of hair recovery area (**e**) and hair-growth cycle score (**f**) at day 28 following treatment. **g** Representative H&E-stained longitudinal sections of skin tissues. Scale bar = 200 μm. **h** Statistical analysis of hair follicle counts in skin tissues on day 28. **i** A pseudo color image of blood flow distribution in mice. **j** Immunofluorescence staining of vascular marker CD31 (red) and follicular activation marker CD34 (green) in skin tissues. Scale bar = 100 μm. Quantitative analysis of FI intensity of $CD31^+$ (**k**) and $CD34^+$ (**l**) on day 28. FI, fluorescence intensity. **c**–**l** AGA, non-stimulated AGA mice. AGA + ES, electrically stimulated AGA mice. **m** Volcano plot of differentially expressed proteins ($n = 3$). **n** GO enrichment analysis chart showing the top 10 significantly enriched pathways ($n = 3$). **o** KEGG enrichment analysis circle chart highlighting the top 10 significantly enriched pathways ($n = 3$). **p** KEGG enrichment analysis circle chart highlighting the top 10 significantly enriched pathways. **q** Western blot analysis of PGM3 and β-catenin protein expression levels. **r** Quantitative analysis of PGM3 and β-catenin protein expression levels. **s** Detection of DHT in skin tissue following different numbers of electrical stimulations. Inflammatory factor levels: **t** TNFα, **u** IL-6, **v** IL-1β. The data were derived from five independent experiments unless otherwise stated and were presented as mean ± SD. A two-sided Student's *t*-test was used for comparisons (**b**, **e**, **f**, **h**, **k**, **l**, **m**–**p**, **r**–**v**). The screening criterion was fold-change >1.2-fold, and $p < 0.05$ was considered statistically significant (**m**–**p**).

both molecules yields the most significant hair-growth outcome among the four groups, achieving a level comparable to that of the surrounding normal skin area (Fig. 4h, i). H&E staining further confirms that dual-molecule delivery results in a significant increase in hair follicles compared to all other groups (Fig. 4j, k). Moreover, dual-molecule delivery outperforms clinical strategies, i.e., oral finasteride (G5) and topical minoxidil (G6), in promoting hair growth and follicle regeneration (Fig. 4f–k).

We next evaluated the efficacy of the dual-molecule delivery group by assessing perifollicular blood vessels and hair follicle stem cell activity. The observed increases in local blood flow, blood vessel density, and the vascular marker CD31 indicated favorable vascular recovery in the dual-molecule delivery group (Fig. 4l–n and Fig. S11). Additionally, elevated levels of the hair follicle stem cell activity marker CD34 suggested robust stem cell activity recovery following dual-molecule delivery (Fig. 4m, o). These results suggest that enhanced vascularization and follicular activity serve as the underlying mechanisms for its superior hair-growth outcomes. Together, these results indicate that the Detangle system-mediated electrostimulation and co-delivery of VEGFA plasmid and SRD5A2 siRNA act synergistically to enhance therapeutic outcomes in AGA.

Mechanism investigation of enhanced AGA treatment by the Detangle system

To elucidate the synergistic mechanism of the Detangle system in AGA treatment, we analyzed the proteins regulated by dual-molecule delivery (VEGFA plasmid and SRD5A2 siRNA) combined with electrostimulation in AGA mice. The analysis reveals that synergistic treatment with Detangle upregulated 632 proteins and downregulated 781 proteins compared to AGA mice, predominantly associated with cellular metabolism (accounting for eight of the top ten enriched terms) (Fig. 5a, b). These enriched terms involve 238 signaling pathways, a number significantly higher than the 227 pathways identified with electrostimulation alone, indicating that the Detangle system synergistically enhances the regulation of cellular metabolic pathways (Fig. 5c). Furthermore, to elucidate the specific signaling pathways involved in this process, three hair-growth-related pathways reported in the literature were evaluated: Wnt/β-catenin signaling pathway, AR signaling pathway, and angiogenic signaling pathway (Fig. S12a, b)[11,37,40,41,45]. The changes of corresponding representative targets β-catenin, AR, and VEGFA confirmed that the Detangle system effectively modulates these key molecules, validating its ability to activate the three major hair-regulatory signaling pathways.

Specifically, in addition to the proteins modulated by electrostimulation alone for improving AGA, the Detangle system, combined with electrostimulation and molecular delivery, further upregulated 15 proteins and downregulated 23 proteins in AGA mice (Fig. 5d–f and Fig. S13a–f). Protein–protein interaction analysis of differentially expressed genes suggests that the VEGFA plasmid upregulates *VEGFA* expression, which further modulates *SRY-box transcription factor 9 (Sox9)* expression, thereby improving perifollicular vascularization and accelerating hair follicle regeneration[46,47]. Concurrently, SRD5A2 siRNA upregulates *sulfotransferase family 2B member 1 (Sult2b1)* by suppressing SRD5A2 expression, thereby attenuating androgen-mediated inhibition of hair follicle activity (Fig. 5g–k)[48]. To investigate whether the enhanced effect stems from a simple additive effect or the crosstalk between signaling pathways, we performed a protein–protein interaction network analysis between VEGFA and SRD5A2 (Fig. S14). The results showed that the enhanced therapeutic effect involves crosstalk between the signaling pathways of these two molecules.

Further analysis shows that key inhibitors of follicular metabolism, including DHT and inflammatory factors, are significantly reduced in the dual-molecule delivery group, reaching levels comparable to those in normal mice (Fig. 5l–o and Fig. S6e, i–k). These results indicate that the Detangle system, through co-delivery of VEGFA plasmid and SRD5A2 siRNA under electrostimulation, effectively modulates cellular metabolism to enhance therapeutic effects on AGA.

Discussion

In this work, we reported Detangle, a daily-use combing system for safe and effective treatment of AGA. The comb teeth, embedded with electrodes of differential height, can generate a directional electric field that penetrates ~9 times deeper than conventional external application during combing. This enhanced penetration allows for the efficient intracellular delivery of regulatory molecules to hair follicle cells and promotes follicle regeneration. By co-delivering VEGFA plasmid and SRD5A2 siRNA, the Detangle system promotes hair follicle regeneration via a dual mechanism that synergizes electrostimulation with molecular regulation. This approach accelerates hair growth nearly 100% within a month in the AGA mouse model, surpassing the outcomes achievable with conventional oral or external medications (~70%). Given the multifaceted signaling abnormalities in AGA, the Detangle system presents a versatile platform for co-delivering therapeutic agents beyond metabolic modulation.

Methods

Fabrication of the Detangle system

The Detangle system consists of a substrate layer, electrode modules, drug-loading modules, and a circuit module. The substrate layer was manufactured via high-precision stereolithography-based 3D printing technology (Shenzhen JLC Technology Group Co., Ltd., China), with its precise dimensional configuration detailed in Fig. S3. The electrode modules are composed of copper rods with a diameter of 1 mm. The drug-loading modules integrate ballpoint pen tips (DL-Bullet1.0, Deli, China) connected to copper wires with a diameter of 0.5 mm. The circuit module was designed using Altium Designer software and subsequently manufactured by Shenzhen JLC Technology Group Co., Ltd. For system assembly, the electrode components of both the electrode and drug-loading modules were first connected to the circuit

https://doi.org/10.1038/s41467-026-79122-3

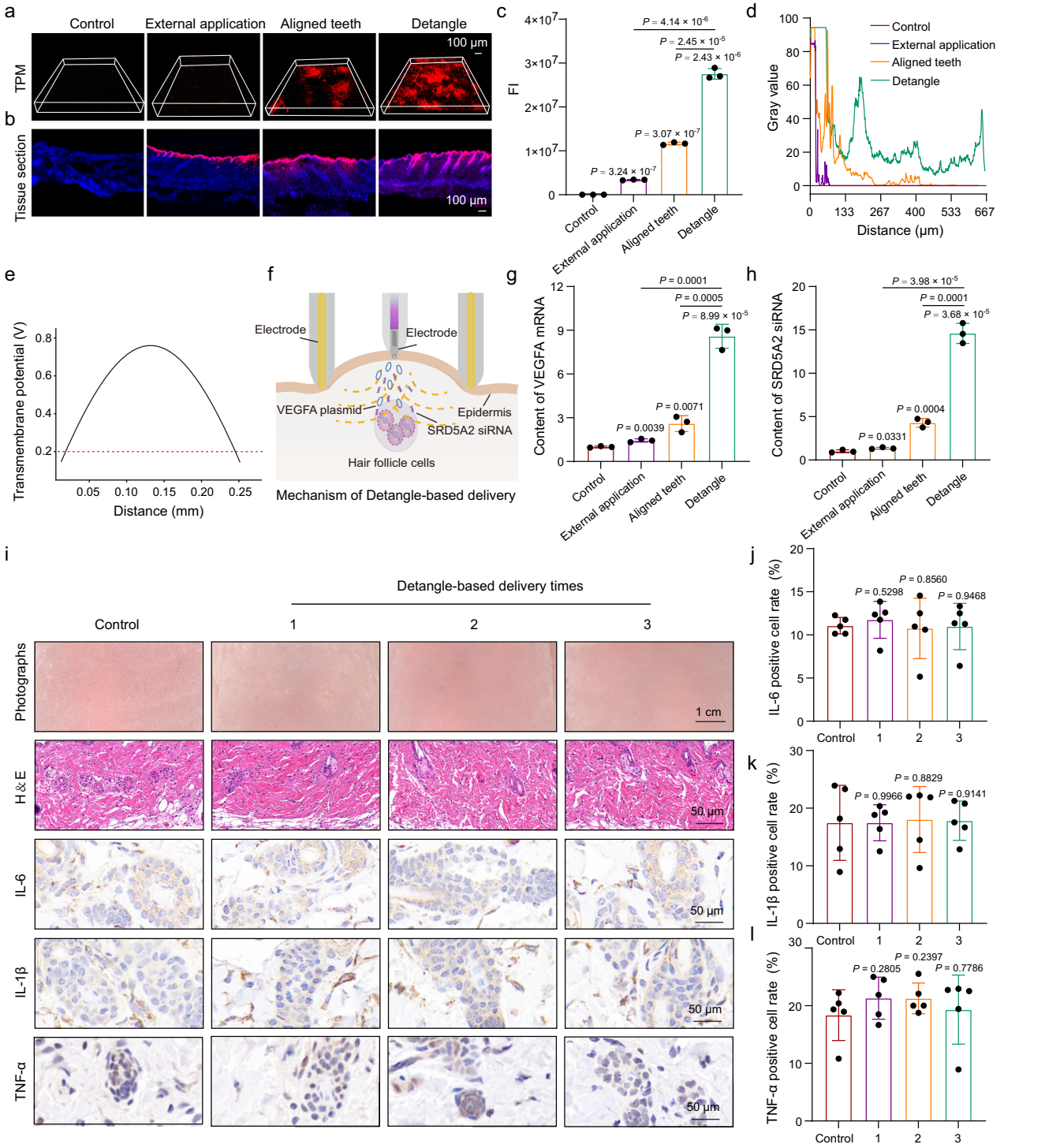


Fig. 3 | Deep molecular delivery by the Detangle system. a Intravital two-photon microscopy (TPM) images showing the efficiency of molecular delivery in skin. Scale bar = 100 μm. **b** Tissue section images showing the depth of molecular delivery in skin. Scale bar = 100 μm. **a**, **b** Propidium iodide was employed as a validation molecule for delivery. **c** Quantitative analysis of fluorescence intensity (**a**) in skin. FI fluorescence intensity. **d** Quantitative analysis of the depth of molecular delivery (**b**) in skin. **e** Transmembrane potentials of deep-layer hair follicle cells under simulated electric field. **f** Schematic of the principle for deep molecular delivery using the Detangle system. **g**, **h** Content analysis of delivered molecules in skin tissue via qPCR. **a**–**h** Control, naive mice without treatment. External application, topical application of molecules. Aligned teeth, the electrical delivery electrodes have no height difference. Detangle delivery, molecule delivery via the Detangle system. **i** Safety assessment of repeated delivery via the Detangle system. Representative photograph demonstrating no signs of adverse skin reactions. Scale bar = 1 cm. H&E, histological images, staining of skin. IL-6, IL-1β, and TNF-α, immunohistochemistry of skin. Scale bar = 50 μm ($n = 5$). Quantitative analysis of inflammatory cytokine-positive cells expression in tissue sections (IL-6 (**j**), IL-1β (**k**), and TNF-α (**l**)). The data were derived from three independent experiments unless otherwise stated and were presented as mean ± SD. A two-sided Student's *t*-test was used for comparisons (**c**, **g**, **h**, **j**–**l**).

https://doi.org/10.1038/s41467-026-79122-3

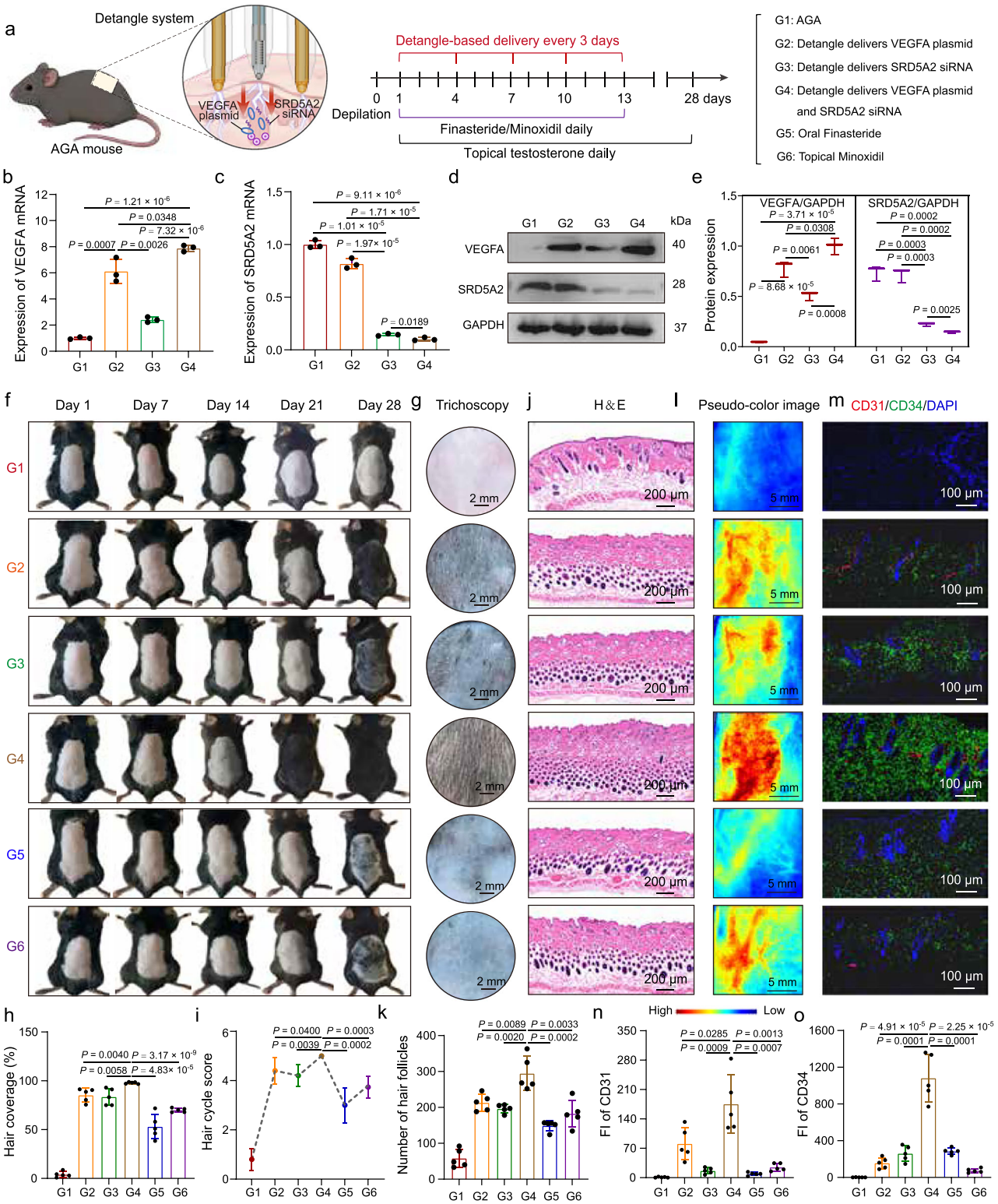


Fig. 4 | Enhanced treatment of AGA via Detangle-mediated deep molecular delivery. a Schematic of the treatment protocol for AGA mouse models using different methods. The AGA mouse model was established by daily topical application of testosterone for 28 consecutive days. Expression levels of *VEGFA* (**b**) and *SRD5A2* (**c**) mRNA after Detangle-mediated molecular delivery ($n = 3$). **d** Western blot analysis of VEGFA and SRD5A2 protein expression levels ($n = 3$). **e** Quantitative analysis of VEGFA and SRD5A2 protein expression levels. **f** Representative photographs showing hair growth in each group from day 1 to day 28. **g** Trichoscopy images of mouse skin tissue from various treatment groups. Scale bar = 2 mm. Comparative quantification of hair recovery area (**h**) and hair-growth cycle score (**i**) on day 28 following treatment. **j** Representative H&E-stained longitudinal sections of skin tissues on day 28. Scale bar = 200 μm. **k** Statistical analysis of hair follicle counts in skin tissues on day 28. **l** A pseudo color image of blood flow distribution in mice. **m** Immunofluorescence staining of follicular-activation markers CD31 (red) and CD34 (green) in skin tissues. Scale bar = 100 μm. Quantitative analysis of FI intensity of $CD31^+$ (**n**) and $CD34^+$ (**o**) cells on day 28. FI, fluorescence intensity. The data were derived from five independent experiments unless otherwise stated and were presented as mean ± SD. A two-sided Student's *t*-test was used for comparisons (**b**, **c**, **e**, **h**, **i**, **k**, **n**, **o**).

https://doi.org/10.1038/s41467-026-79122-3

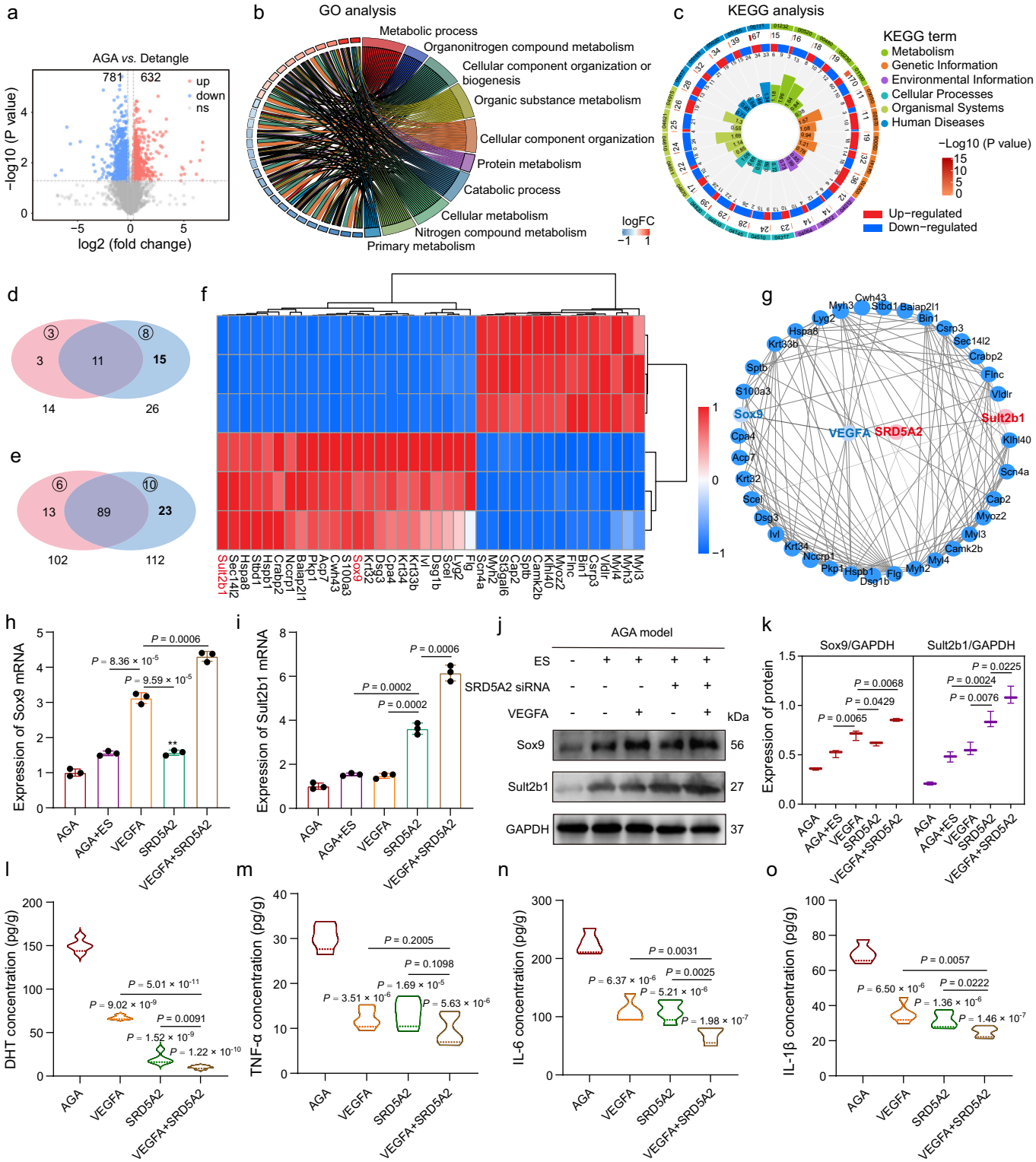


Fig. 5 | Mechanism of enhanced AGA treatment through synergistic electrostimulation and molecular delivery in the Detangle system. a A volcano plot of differentially expressed proteins in AGA mice *vs.* AGA mice treated with the Detangle system. **b** GO enrichment analysis chart showing the top 10 significantly enriched pathways. **c** KEGG enrichment analysis circle chart highlighting the top 10 significantly enriched pathways. Venn diagrams showing upregulated (**d**) and downregulated (**e**) proteins in the dual-molecule delivery group compared to the electrostimulation group. The left circles respectively represent the numbers of upregulated (**d**, ③) and downregulated (**e**, ⑥) proteins that overlap between genes abnormally expressed in AGA mice and genes regulated by electrostimulation treatment. The right circles respectively represent the numbers of upregulated (**d**, ⑧) and downregulated (**e**, ⑩) proteins that overlap between genes abnormally expressed in AGA mice and genes regulated by dual-molecule delivery. Overlapping segments indicate the number of regulated proteins shared between the two groups. **f** Proteins exclusively regulated by the Detangle system-mediated dual-molecule delivery. **g** Protein interaction network diagram of regulatory molecules with the proteins in (**f**). Analysis of *Sox9* (**h**) and *Sult2b1* (**i**) mRNA expression levels. **j** Western blot analysis of Sox9 and Sult2b1 protein expression levels. **k** Quantitative

module. These integrated components were then assembled into the substrate layer. Next, the molecules to be delivered were dissolved in PBS, loaded into the cavity of the drug-loading modules, and sealed with 200 μL paraffin liquid (8042-47-5, Aladdin, China). Finally, the substrate layer was fully assembled to complete the Detangle system.

Establishment of the AGA mouse model

Male C57BL/6 mice aged five to six weeks were chosen for establishing the AGA experimental model, given their consistent androgen background and easily distinguishable hair-regrowth phenotypes. These animals were acquired from the SPF Laboratory Animal Technology (Beijing, China, Animal Certification No. SCXK 2019-0010) and housed inside isolated cage units within a pathogen-free animal facility. Every animal-related procedure received ethical clearance from the Experimental Animal Welfare Ethics Committee of Beijing Chest Hospital, Capital Medical University (approval identifier XK2024-124). All manipulations strictly complied with standardized laboratory-animal care specifications and humane-treatment guidelines for experimental animals.

To generate the AGA pathological phenotype, the dorsal fur of each mouse was first mechanically shaved, and residual hair was fully eliminated using depilatory cream.

Subsequently, testosterone solution (0.2% w/v, GC45935, GLPBIO, USA) prepared in 50% (v/v) ethanol (CAS 64-17-5, National Pharmaceutical Reagents, China) was applied topically to the depilated area once daily at a dose of 0.1 mL/cm² for a total of 28 consecutive days[5,11,41,49].

Treatment of AGA mouse

For AGA mouse treatment by the Detangle system, therapeutic payloads including 5 μg VEGFA plasmid and 20 nM si-SRD5A2 were loaded into the drug-loading modules (Table S1). The depilated area was treated with the Detangle system every three days, using electrical parameters of 30 V, 1 ms pulse duration, 10 Hz pulse frequency, and 100 pulses per session[21,50]. For the oral administration, finasteride (CAS 98319-26-7, GLPBIO, USA) was incorporated into mouse feed at a dose of 1.5 mg per 30 g body weight. For topical administration, 5% minoxidil solution (CAS 38304-91-5, GLPBIO, USA) was applied daily to the depilated area at a dose of 0.2 mL. Hair growth in mice was monitored at days 1, 7, 14, 21, and 28 post-treatment.

Once experimental endpoints were reached, animals were humanely euthanized. After dorsal fur removal and surface disinfection using 75 % ethanol, full-thickness skin specimens covering both epidermal and dermal compartments were rapidly excised from target regions with pre-chilled sterile surgical instruments. Collected tissues were rinsed in ice-cold RNase-free PBS buffer to wash away surface blood contaminants, and residual moisture was gently blotted with sterile filter paper for subsequent analysis.

Hair-growth assessment

To evaluate hair growth following a 28-day treatment, hair coverage was measured using the ImageJ FIJI software. Additionally, skin condition and hair-growth cycle were scored following a standardized grading rubric: Score 0 – No observable hair growth, depilated area presents a pink appearance; Score 1 – Gray-hued skin on depilated sites, with regenerated hair covering less than 20 % of the area; Score 2 – Black-pigmented skin on depilated sites, hair-regrowth proportion ranging from 20 % to 40 %; Score 3 – Black-pigmented skin with sparse new hair, covering 40–60 % of the measured region; Score 4 – Black-pigmented skin together with partial hair regrowth, covering 60–80 % of the depilated area; Score 5 – Near-complete hair restoration, with 80–100 % area covered by regenerated hair[51–53].

Histological staining

Skin samples collected from the depilated area of mice were fixed overnight within 4% paraformaldehyde solution (G1101, Servicebio, China). Fixed samples then underwent paraffin embedding, followed by sectioning to generate 10-μm-thick frozen tissue slices. Prior to staining, paraffin-embedded sections went through sequential dewaxing and hydration steps. Hematoxylin-eosin coloration was then carried out adopting a commercial staining kit (G1076, Servicebio, China), following the manufacturer-supplied operating protocols. Subsequently, the samples were observed and analyzed under a microscope.

Immunofluorescence histochemistry

The immunofluorescent labeling was implemented utilizing the double antibody-Tyramide signal amplification (TSA) method. This experimental procedure consisted of primary-antibody incubation, secondary-antibody binding, and TSA signal amplification (Table S2). Subsequently, DAPI reagent (GDP1024, Servicebio, China) was applied for nuclear counterstaining. Processed glass slides were then imaged under a fluorescence microscope (CKX3-SLP, OLYMPUS, Japan).

Proteomics analysis

To explore the impacts of electrostimulation and molecular delivery on hair growth, total protein molecules were isolated from collected skin samples, followed by proteome profiling performed via nanoLC-MS/MS technology (Biotree, China). Proteins exhibiting fold-change >1.2-fold and $p < 0.05$ were regarded as statistically meaningful differentially expressed candidates. *P*-value computation relied on Fisher's exact test, built upon the hypergeometric distribution. For multiple-comparison correction, the Benjamini–Hochberg adjustment approach was adopted. In KEGG enrichment analysis (Fig. 2o and Fig. 5c), the outermost ring (Ring 1) corresponds to functional categories from gene-ontology resources, with color coding and scale bars reflecting protein counts. Ring 2 exhibits data for differentially enriched genes: bar length correlates with the number of altered proteins, and color intensity represents −log10 (*p*-value). Ring 3 visualizes up-regulation (red) versus down-regulation (blue) ratios for differential molecules. The innermost Ring 4 displays enrichment scores calculated as log2 (Fold Enrichment).

Enzyme-linked immunosorbent assay (ELISA)

ELISA was deployed to quantify key biomolecules that mediate follicular metabolic suppression within skin tissue specimens. All experimental manipulations strictly followed operational guidelines supplied by corresponding commercial assay kits, including DHT ELISA kit (E-EL-0031, Elabscience Biotechnology, China), IL-6 ELISA kit (E-EL-M0044, Elabscience Biotechnology, China), IL-1β ELISA kit (E-EL-M0037, Elabscience Biotechnology, China), as well as TNF-α ELISA kit (E-EL-M3063, Elabscience Biotechnology, China). Briefly, harvested skin samples underwent homogenization and lysis procedures to release intracellular components. Supernatant fractions were separated through centrifugation steps. A bicinchoninic acid (BCA) protein quantification kit (ZJ102, Epizyme Biotechnology, China) was utilized to determine total protein concentrations within each supernatant aliquot. Subsequently, sample lysates were split into three separate portions for targeted biomarker measurement by a microplate reader (Spark, TECAN, Switzerland).

RNA extraction and RT-qPCR assay

Total ribonucleic acid was isolated from mouse skin samples by adopting a commercial RNA extraction kit (RC112, Vazyme, China), with all experimental steps carried out as stated within the product manual. RT-qPCR was then implemented with the HiScript II One-Step qRT-PCR SYBR Green kit (Q221, Vazyme, China) to quantify transcript

abundance of target genes. Sequences for all primers applied in this study were compiled in Table S1.

Western blot analysis

Total protein was liberated from tissue specimens using RIPA lysis buffer (PC101, Epizyme Biotechnology, China). After lysis completion, the BCA assay was conducted to determine protein concentration for each sample aliquot. Protein fractions were separated electrophoretically on 12.5% polyacrylamide gel (PG113, Epizyme Biotechnology, China), followed by electrophoretic transfer onto polyvinylidene difluoride membranes (88518, ThermoFisher, USA). Membrane blocking was completed with 5% bovine serum albumin (BSA, PS113, Epizyme Biotechnology, China) dissolved in TBST (TBS supplemented with 0.1% Tween-20, PS103, Beyotime Biotechnology, China). Blocked membranes were incubated with primary antibody overnight under 4 °C conditions (Table S2). After repeated TBST washing cycles, membranes were further incubated with HRP-tagged secondary antibody for 40 min at room temperature. The protein bands were then visualized via a chemiluminescence imaging system (GE Healthcare, UK).

Statistical analysis

A simplified computational model for the Detangle apparatus was built within COMSOL Multiphysics software (Version 6.1) to simulate the spatial electric-field distribution. Data were processed and analyzed using Origin 8.0, GraphPad Prism 9.0, and ImageJ FIJI software. Two-tailed Student's *t*-test and one-way analysis of variance (ANOVA) served as statistical comparison approaches throughout this study. All quantitative outputs are presented in the format of mean values paired with standard deviation (SD). Statistical significance was designated whenever computed p-values fell below the threshold of 0.05.

Reporting summary

Further information on research design is available in the Nature Portfolio Reporting Summary linked to this article.

Data availability

The transcriptome sequencing raw data reported in this paper have been deposited in the Genome Sequence Archive in the National Genomics Data Center under the accession number "CRA038375 [https://ngdc.cncb.ac.cn/gsa/browse/CRA038375]". The mass spectrometry proteomics data have been deposited to the ProteomeXchange Consortium via the iProX partner repository with the dataset identifier "PXD074222 [https://www.iprox.cn/page/project.html?id=IPX0015674000]". Any additional requests for information can be directed to and will be fulfilled by the corresponding authors. Source data are provided with this paper.

References

1. Devjani, S., Ezemma, O., Kelley, K. J., Stratton, E. & Senna, M. Androgenetic alopecia: therapy update. *Drugs* **83**, 701–715 (2023).
2. Oiwoh, S. O., Enitan, A. O., Adegbosin, O. T., Akinboro, A. O. & Onayemi, E. O. Androgenetic alopecia: a review. *Niger. Postgrad. Med. J.* **31**, 85–92 (2024).
3. Xiao, Y., Zhang, Y., Deng, S., Yang, X. & Yao, X. Immune and non-immune interactions in the pathogenesis of androgenetic alopecia. *Clin. Rev. Allergy Immunol.* **68**, 22 (2025).
4. Cao, Z. et al. Erythrocyte extracellular vesicles amalgamate into the hair and skin to maintain homeostasis. *J. Extracell. Vesicles* **14**, e70080 (2025).
5. Gupta, A. K., Talukder, M. & Williams, G. Comparison of oral minoxidil, finasteride, and dutasteride for treating androgenetic alopecia. *J. Dermatol. Treat.* **33**, 2946–2962 (2022).
6. Gupta, A. K. & Talukder, M. Topical finasteride for male and female pattern hair loss: Is it a safe and effective alternative? *J. Cosmet. Dermatol.* **21**, 1841–1848 (2022).
7. Sadeghzadeh Bazargan, A. et al. The efficacy of the combination of topical minoxidil and oral spironolactone compared with the combination of topical minoxidil and oral finasteride in women with androgenic alopecia, female and male hair loss patterns: a blinded randomized clinical trial. *J. Cosmet. Dermatol.* **23**, 543–551 (2024).
8. Fazal, F. et al. Can oral minoxidil be the game changer in androgenetic alopecia? A comprehensive review and meta-analysis comparing topical and oral minoxidil for treating androgenetic alopecia. *Skin Health Dis.* **5**, 95–101 (2025).
9. Jing, S. et al. Microneedle-mediated hypoxic extracellular vesicle-encapsulated selenium nanoparticles delivery to treat androgenetic alopecia. *J. Control. Release* **381**, 113597 (2025).
10. Younis, N. et al. Microneedle-mediated delivery of immunomodulators restores immune privilege in hair follicles and reverses immune-mediated alopecia. *Adv. Mater.* **36**, e2312088 (2024).
11. Chen, Y. et al. Gas-propelled anti-hair follicle aging microneedle patch for the treatment of androgenetic alopecia. *J. Control. Release* **379**, 636–651 (2025).
12. Xu, S., Zhou, L., Zhao, H. & Li, S. Advances in transdermal delivery systems for treating androgenetic alopecia. *Pharmaceutics* **17**, 984 (2025).
13. Wang, R. et al. PROTAC degraders of androgen receptor-integrated dissolving microneedles for androgenetic alopecia and recrudescence treatment via single topical administration. *Small Methods* **7**, e2201293 (2023).
14. Singh, R. et al. Alopecia areata: review of epidemiology, pathophysiology, current treatments and nanoparticulate delivery system. *Ther. Deliv.* **15**, 193–210 (2024).
15. Tian, J. B. et al. TRPC4 and GIRK channels underlie neuronal coding of firing patterns that reflect G(q/11)-G(i/o) coincidence signals of variable strengths. *Proc. Natl. Acad. Sci. USA* **119**, e2120870119 (2022).
16. Wu, H. et al. Electrical stimulation of piezoelectric BaTiO3 coated Ti6Al4V scaffolds promotes anti-inflammatory polarization of macrophages and bone repair via MAPK/JNK inhibition and OXPHOS activation. *Biomaterials* **293**, 121990 (2023).
17. Wang, T. et al. Rehabilitation exercise-driven symbiotic electrical stimulation system accelerating bone regeneration. *Sci. Adv.* **10**, eadi6799 (2024).
18. Jellard, S., Moore, S. & Chacon-Martinez, C. A. Novel electrotrichogenic device promotes hair growth in men with androgenetic alopecia: a pilot study. *J. Cosmet. Dermatol.* **24**, e70202 (2025).
19. Yao, G. et al. Self-activated electrical stimulation for effective hair regeneration via a wearable omnidirectional pulse generator. *ACS Nano* **13**, 12345–12356 (2019).
20. Martinez-Pascual, M. A., Sacristan, S., Toledano-Macias, E., Naranjo, P. & Hernandez-Bule, M. L. Effects of RF electric currents on hair follicle growth and differentiation: a possible treatment for alopecia. *Int. J. Mol. Sci.* **25**, 7865 (2024).
21. Yin, D. et al. A battery-free nanofluidic intracellular delivery patch for internal organs. *Nature* **642**, 1051–1061 (2025).
22. Xiao, A. et al. A degradable bioelectronic scaffold for localized cell transfection toward enhancing wound healing in a 3D space. *Adv. Mater.* **36**, e2404534 (2024).
23. Liu, F. et al. Advanced micro/nano-electroporation for gene therapy: recent advances and future outlook. *Nanoscale* **16**, 10500–10521 (2024).
24. Kageyama, T., Seo, J., Yan, L. & Fukuda, J. Effects of oxytocin on the hair growth ability of dermal papilla cells. *Sci. Rep.* **13**, 15587 (2023).
25. Xiong, S. et al. Black phosphorus nanosheets encapsulated microneedle for multifunctional therapy for androgenic alopecia. *J. Nanobiotechnology* **23**, 147 (2025).

26. Wang, Z., Gu, B., Sharkey, C., Ge, R. & Olumi, A. F. SRD5A2 and emerging therapies in androgen-driven disorders. *Nat. Rev. Urol.* **23**, 319–332 (2026).
27. Nestor, M. S., Ablon, G., Gade, A., Han, H. & Fischer, D. L. Treatment options for androgenetic alopecia: Efficacy, side effects, compliance, financial considerations, and ethics. *J. Cosmet. Dermatol.* **20**, 3759–3781 (2021).
28. Zhu, D., Liu, D., Wu, K., Cheng, X. & Yang, Y. GPR87 promotes angiogenesis in esophageal squamous cell carcinoma via VEGFA regulation. *Mol. Carcinog.* **64**, 1057–1065 (2025).
29. Chan, A. O. et al. Diagnosis of 5alpha-reductase 2 deficiency: is measurement of dihydrotestosterone essential? *Clin. Chem.* **59**, 798–806 (2013).
30. Liu, F. et al. A nano-electro-platform enabling evolutionary screening and remodeling of tumor cells for metastasis inhibition. *Adv. Sci.* **12**, e07684 (2025).
31. Dong, Z. et al. Genetic and phenotypic profiling of single living circulating tumor cells from patients with microfluidics. *Proc. Natl. Acad. Sci. USA* **121**, e2315168121 (2024).
32. Miller, I. et al. Ki67 is a graded rather than a binary marker of proliferation versus quiescence. *Cell Rep.* **24**, 1105–1112.e1105 (2018).
33. Dumitru, I. et al. Identification of proliferating neural progenitors in the adult human hippocampus. *Science* **389**, 58–63 (2025).
34. Nadal-Nicolas, F. M. et al. Pan-retinal ganglion cell markers in mice, rats, and rhesus macaques. *Zool. Res.* **44**, 226–248 (2023).
35. Tavares-Ferreira, D. et al. Spatial transcriptomics of dorsal root ganglia identifies molecular signatures of human nociceptors. *Sci. Transl. Med.* **14**, eabj8186 (2022).
36. Greiner, G. et al. Hereditary alpha tryptasemia is a valid genetic biomarker for severe mediator-related symptoms in mastocytosis. *Blood* **137**, 238–247 (2021).
37. Sun, Y. et al. HDAC1-overexpressing dermal papilla cell-derived extracellular vesicles modulate p53 and Wnt/beta-catenin signaling to rescue hair follicle regeneration in androgenetic alopecia. *Biomaterials* **329**, 123969 (2026).
38. Yuan, A. et al. Ceria nanozyme-integrated microneedles reshape the perifollicular microenvironment for androgenetic alopecia treatment. *ACS Nano* **15**, 13759–13769 (2021).
39. Hu, X. et al. Self-assembling peptide inspired by insulin and type 1 insulin-like growth factor for the treatment of androgenetic alopecia. *Bioact. Mater.* **53**, 819–830 (2025).
40. Ding, Y. W., Li, Y., Zhang, Z. W., Dao, J. W. & Wei, D. X. Hydrogel forming microneedles loaded with VEGF and Ritlecitinib/polyhydroxyalkanoates nanoparticles for mini-invasive androgenetic alopecia treatment. *Bioact. Mater.* **38**, 95–108 (2024).
41. Bai, L. et al. Materiobiomodulated ROS therapy for de novo hair growth. *Adv. Mater.* **36**, e2311459 (2024).
42. Zhang, N. et al. PGM3 regulates beta-catenin activity to promote colorectal cancer cell progression. *Exp. Biol. Med.* **247**, 1518–1528 (2022).
43. Chen, D. et al. Fibroblast bioelectric signaling drives hair growth. *Cell* **188**, 5175–5193.e5121 (2025).
44. Han, B. et al. Differences of adrenal-derived androgens in 5alpha-reductase deficiency versus androgen insensitivity syndrome. *Clin. Transl. Sci.* **15**, 658–666 (2022).
45. Yan, R., Cui, W., Cheng, X., Li, J. & Lin, Y. Sustainability of functional hair follicle activity: Impact of spatially anchored multifunctional tetrahedral framework nucleic acids. *Bioact. Mater.* **57**, 344–357 (2026).
46. Zou, J. et al. Notch1 signaling regulates Sox9 and VEGFA expression and governs BMP2-induced endochondral ossification of mesenchymal stem cells. *Genes Dis.* **12**, 101336 (2025).
47. Chen, Y. et al. Lipid nanoparticle-encapsulated VEGFa siRNA facilitates cartilage formation by suppressing angiogenesis. *Int. J. Biol. Macromol.* **221**, 1313–1324 (2022).
48. Lu, B., et al. Genetic basis and evolutionary forces of sexually dimorphic color variation in a toad-headed agamid lizard. *Mol. Biol. Evol.* **41**, msae054 (2024).
49. Cao, S. et al. Microneedles mediated bioinspired lipid nanocarriers for targeted treatment of alopecia. *J. Control. Release* **329**, 1–15 (2021).
50. Wang, Y. et al. An organ-conformal, kirigami-structured bioelectronic patch for precise intracellular delivery. *Cell* **189**, 1086–1107.e1032 (2026).
51. Yan, W. et al. Restoration of follicular beta-catenin signaling by mesenchymal stem cells promotes hair growth in mice with androgenetic alopecia. *Stem Cell Res. Ther.* **15**, 439 (2024).
52. Feng, D. et al. Efficient silencing of androgen receptor gene via UTR-targeting siRNAs for androgenetic alopecia therapy. *J. Med. Chem.* **68**, 20586–20594 (2025).
53. Wang, Z. et al. Fucoidan treatment reverses hair loss and inhibits inflammatory responses in a mouse model of androgenetic alopecia. *Int. J. Biol. Macromol.* **322**, 146382 (2025).

Author contributions

L.C., Z.D., and Y.J. led the whole project. L.C. and Y.J. conceived the Detangle system. Z.D. designed the use of the Detangle system for hair growth. F.L. led the experiments and conducted the in vivo mouse experiments. F.Y. and H.S. verified the specific application of the Detangle system. C.W., B.L., C.D., H.W., R.Z. and N.W. assisted with the in vivo mouse experiments. Y.T., D.Y., X.X., T.F., L.L., and P.Z. assisted with the specific application of the Detangle system. L.C., Z.D. and F.L. co-wrote the paper.

Funding

This work was supported by the following fundings: National Science Fund for Distinguished Young Scholars (No. T2425021), National Natural Science Foundation of China (Nos. T25B2018, T24B2006, 22304006, 62471021, 82303583), the Fundamental Research Funds for the Central Universities (Nos. JKF-2025082276817, JKF-20240574), Shandong Provincial Natural Science Foundation (Nos. ZR2024QB014, ZR2024QF010), the Academic Excellence Foundation of BUAA for PhD Students.

Competing interests

The authors declare no competing interests.

Additional information

Supplementary information The online version contains supplementary material available at https://doi.org/10.1038/s41467-026-79122-3.

Correspondence and requests for materials should be addressed to Yanli Jiao, Zaizai Dong or Lingqian Chang.

Peer review information *Nature Communications* thanks Ramon Grimalt and the other, anonymous, reviewers for their contribution to the peer review of this work. A peer review file is available.

Reprints and permissions information is available at http://www.nature.com/reprints

Publisher's note Springer Nature remains neutral with regard to jurisdictional claims in published maps and institutional affiliations.

Open Access This article is licensed under a Creative Commons Attribution-NonCommercial-NoDerivatives 4.0 International License, which permits any non-commercial use, sharing, distribution and reproduction in any medium or format, as long as you give appropriate credit to the original author(s) and the source, provide a link to the Creative Commons licence, and indicate if you modified the licensed material. You do not have permission under this licence to share adapted material derived from this article or parts of it. The images or other third party material in this article are included in the article's Creative Commons licence, unless indicated otherwise in a credit line to the material. If material is not included in the article's Creative Commons licence and your intended use is not permitted by statutory regulation or exceeds the permitted use, you will need to obtain permission directly from the copyright holder. To view a copy of this licence, visit http://creativecommons.org/licenses/by-nc-nd/4.0/.

© The Author(s) 2026

This Article in Press is shared early to give you faster access to new research. It is citable and carries a permanent DOI. The final edited version will replace it automatically.